Okhotsk Sea and Polar Oceans Research 4 (2020) 1-9

https://doi.org/10.57287/ospor.4.1

Article

Storm–mediated ocean–atmosphere heat exchange over the Arctic Ocean: A case study of a Barents Sea cyclone observed in January 2011

Atsuyoshi MANDA[1], Taku MITSUI[2], Jun INOUE[2, 3], Masatake E. HORI[3, 4], Kazuaki KAWAMOTO[5] and Kensuke K. KOMATSU[1]

[1] *Mie University*, *Tsu*, *Japan*
[2] *The Graduate University for Advanced Studies*, *SOKENDAI*, *Tachikawa*, *Japan*
[3] *National Institute of Polar Research, Tachikawa*, *Japan*
[4] *Japan Agency for Marine-Earth Science and Technology*, *Yokosuka, Japan*
[5] *Nagasaki University*, *Nagasaki*, *Japan*

(Received September 9, 2019; Revised manuscript accepted November 19, 2019)

Abstract

Recent studies indicated the importance of cyclones in terms of Arctic warming. Most previous literature has focused on horizontal latent and sensible heat transport from lower latitudes and paid little attention to the effect of surface evaporation in the Arctic Ocean. We here examine the effects of surface evaporation on the lifecycle of a cyclone and thermodynamic structure around a cyclone by conducting a series of numerical simulations, carefully validated with shipboard surface meteorological observations and atmospheric soundings. Although the atmospheric environment and development mechanism of the cyclone are quite different from those of tropical cyclone, the surface fluxes play a role in the life cycle of the cyclone. Enhanced surface evaporation over the Nordic Seas contributes to the longevity of the cyclone, and the effect of evaporation is comparable to that of the surface sensible heat flux. An increase in moisture due to surface evaporation results in atmospheric warming in the lower troposphere over the Barents Sea, mainly because of local condensational and boundary layer heating, and the advection of warm air, which is presumably caused by modification of the air mass around the cyclone. The recent sea-ice decline and associated enhanced evaporation potentially intensify such storm-mediated atmospheric heat-exchange and lead to further Arctic warming.

Key words: cyclone; Barents Sea; air–sea interaction; surface heat flux; Arctic amplification

1. Introduction

Cyclones are an important component of the Arctic climate system (Serreze, 1995). They crucially affect the energy balance of the polar region by transporting huge amounts of heat and moisture (Zahn et al., 2018). In some extreme cases, intense cyclones generate large anomalous warming over the Arctic (e.g., Moore, 2016). Cyclones also affect the concentration and melting of sea ice (Boisvert et al., 2016) and thus control the atmospheric energy supply from the surface. Hence, any changes in cyclone activity directly affect the Arctic energy balance (Zahn et al., 2018).

A recent study showed a coherent interannual variation of moisture transport from lower latitudes and air temperature during winter (Hao et al., 2019). Dufour (2016) showed that transient eddies provide the bulk of the imported mid-latitude moisture (~90% at 70°N), which suggests the importance of cyclones in recent Arctic warming. Meanwhile, surface fluxes play an important role in Arctic warming, especially in the lower troposphere (Screen et al., 2010; Deser et al., 2010; Dai et al., 2019). Strong winds over the ice-free ocean surface associated with cyclones can intensify surface fluxes, which affects the lifecycle of cyclones and in turn atmospheric warming. Adakudlu and Barstad (2011) documented that their modelled cyclone had a prolonged phase of a surface low at its peak intensity when they removed sea ice around Svalbard. Kolstad et al. (2016) showed that surface heat fluxes intensify the mature phase of a polar low and warming in the lower troposphere. Such storm-mediated ocean–atmosphere heat exchange was suggested by Inoue and Hori (2011). However, its detailed process has not been fully examined and is thus not yet fully understood.

In January 2011, we made shipboard atmospheric soundings and surface meteorological observations in the Barents Sea and successfully observed a marine cyclone, which remained around the sea-ice edge in the Barents Sea and may have affected the atmospheric

thermodynamic structure. The present study elucidates the effect of surface evaporation on the lifecycle of this cyclone and the storm-mediated heat exchange process through a series of numerical simulations. Although surface evaporation is not large over the Arctic Ocean, compared to lower latitudes, it has a long-term increasing trend (Boisvert et al., 2015), and the results of the present study will thus shed light on recent Arctic warming and contribute to its future projection.

The remainder of the paper is organized as follows. The data and method used in the study are described in Section 2. Section 3 documents the results of numerical simulations. A summary and discussion are provided in Section 4.

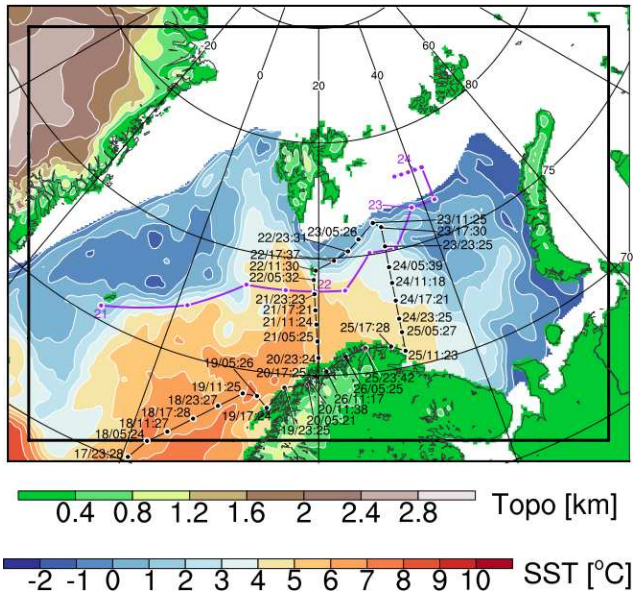

Fig. 1 Map showing the topography (Topo) and SST field derived from OISST on 21 January 2011 in the study area. Overlaid on the SST field are black lines and circles, respectively indicating ship transects and locations of shipboard sounding stations. Numerals with slashes and colons indicate the day of the month and the UTC time (e.g., 21/12:15 represents 12:15 UTC on 21 January 2011) of the sounding. Purple lines with circles represent the tracks of the cyclone estimated from ERA-Interim data; two-digit numbers indicate the day of the month (time is 00:00 UTC). The rectangle with thick black lines marks the domain of the numerical simulations.

2. Data and method

2.1 In situ observations

A joint survey of the Arctic ocean–atmosphere system was conducted by the Japan Agency for Marine–Earth Science and Technology and the Institute of Marine Research in Norway from 13 to 26 January 2011 on board the research vessel (R/V) Johan Hjort of the Institute of Marine Research. Figure 1 shows the locations of sounding stations overlaid on the sea-surface temperature (SST) field. For brevity, we abbreviate times as the day of the month in January 2011 and the UTC time, such that 21/12:15 represents 12:15 UTC on 21 January 2011. On board the ship, we used radiosondes (Vaisala RS92-SGPD) to measure air temperature, relative humidity (RH), and wind velocity every 1 s from the sea surface to approximately 15 km above the sea surface. Surface marine meteorological observations of the SST, surface air temperature (SAT), sea-level pressure (SLP), surface wind velocity, and RH were available at 1-min intervals. We used WindObserver II (Gill Instruments) for surface wind velocity, PTB220 (Vaisala) for SLP, HMP45D (Vaisala) for SAT and RH, SBE-3 (Sea-Bird Electronics) for SST. These in situ data were neither assimilated into the reanalysis dataset nor used in the numerical simulations. They were considered as independent data and used to evaluate the model performance in reproducing atmospheric fields during the survey.

2.2 Atmospheric model

We conducted numerical simulations to elucidate the roles of surface evaporation in the lifecycle of the observed cyclone and atmospheric warming. Version 3.5.1 of the polar-optimized Weather Research and Forecasting model (Polar WRF) developed by Hines and Bromwich (2008) was used in the simulations. Readers are referred to Skamarock et al. (2008) for the specifications of an original version of the model. The land surface model has been optimized for the Arctic climate and well validated using various observational data (Hines and Bromwich, 2008). The model domain is indicated by the rectangle with thick black lines in Figure 1. The horizontal grid spacing was set to 10 km and the model had 50 vertical levels up to 10 hPa. We used five parameterization schemes: the Morrison two-moment scheme (Morrison et al., 2009) for cloud microphysics, Mellor–Yamada–Nakanishi–Niino scheme (Nakanishii and Niino, 2009) for turbulence closure, new Kain–Fritsch scheme (Kain, 2004) for cumulus convection, Dudhia shortwave scheme (Dudhia 1989), and a rapid radiative transfer model (Mlawer et al., 1997) for radiation. The Yonsei University scheme (Hong et al., 2006) was also tested, but the model output varied little for different parametrizations. Optimum Interpolation Sea Surface Temperature (OISST; Reynolds et al., 2007) data were used for the bottom boundary condition over the sea surface. European centre for medium-range weather forecasts interim reanalysis (ERA-Interim; Dee et al. 2011) was employed for the initial and boundary conditions of other prognostic variables.

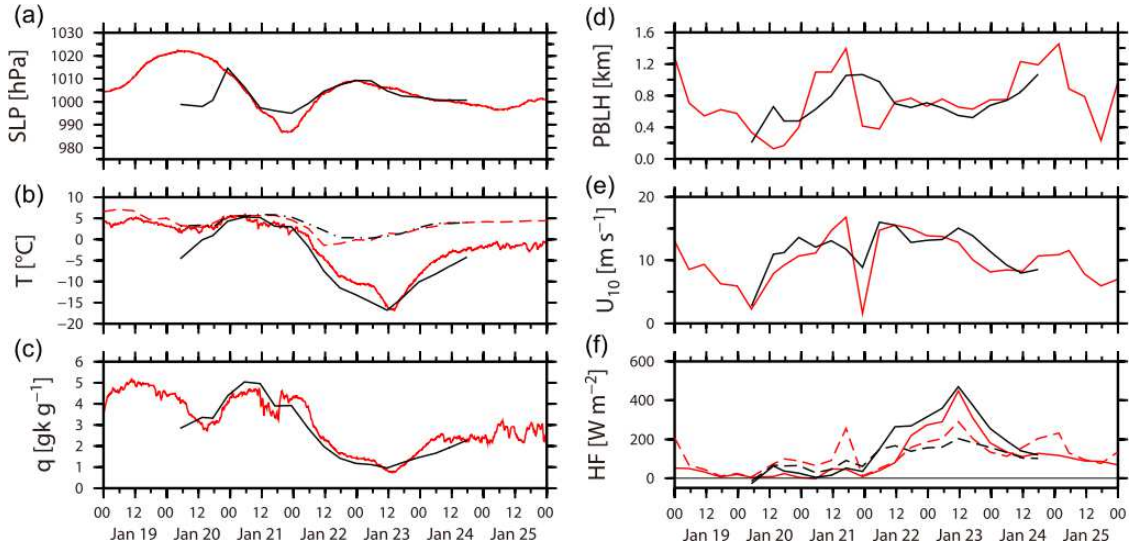

Fig. 2 Comparison of time series of shipboard surface meteorological observations (red) and CNTL (black). (a) SLP, (b) SAT (solid), shipboard measured SST (dot-dashed), and OISST (dashed), (c) surface specific humidity, (d) PBLH, (e) U_{10}, and (f) SHF (solid) and LHF (dashed) along the ship transect (black lines and circles in Fig. 1).

2.3 Numerical experiments

A series of numerical experiments were conducted to examine the roles of surface fluxes in the development and maintenance of a cyclone. A full-physics control model simulation (CNTL) was conducted to reproduce the life cycle of the observed cyclone. The time integration of CNTL started at 21/00:00 and ended at 25/00:00. The relative importance of various physical processes changes during the life cycle of the cyclone and the removal of a certain physical process changes the environment in which the cyclone develops (Føre et al., 2012). Shutting off the physical processes from the development phase makes the interpretation of the results during the mature phase difficult. Thus, two groups of sensitivity experiments with different periods of time integration were designed, following Føre et al. (2012). Time integration in one group of experiments including, no turbulent heat flux (NoTF), no sensible heat flux (NoSF), and no evaporation (NoEV) experiments started at 21/00:00 and ended at 22/00:00, focusing on a development phase of the cyclone. Another group denoted by the capital letter D (delayed) at the end of the abbreviation (NoTF-D, NoSF-D, NoEV-D) focused on the mature phase and began at 22/00:00 and ended at 25/00:00. The initial conditions of these delayed experiments were taken as the output of CNTL at 22/00:00 using the restart functionality of the WRF model. Both surface sensible heat flux and evaporation were turned off in NoTF and NoTF-D. In NoSF and NoSF-D, only the surface sensible heat flux was shut off. In NoEV and NoEV-D, only the surface evaporation was switched off. To compare the relative importance of the surface fluxes with condensational heating, we conducted additional sensitivity experiments (NoMC and NoMC-D), in which both the cloud microphysics and cumulus schemes were shut off.

3. Results

3.1 Model validation

Figure 2 compares surface meteorological observations with model outputs of CNTL. Although the model underestimated the observed SLP minima at around 20/12:00 and 22/00:00, it reproduced temporal variations of SLP correctly. Model output was also in agreement with observations for the SAT, surface specific humidity, planetary boundary layer height (PBLH), wind speed at a height of 10 m (U_{10}), sensible heat flux (SHF), and latent heat flux (LHF).

Model results were further compared with in situ atmospheric soundings (Fig. 3). From 20/00:00 to 21/18:00, in situ atmospheric soundings recorded large RH values from the lower to upper troposphere, suggesting horizontal moisture transport. The tropopause then started to fall from 21/12:00, indicating cyclone development. The wind became strong and veered from southwesterly to northwesterly from 21/12:00 to 22/12:00. This indicated the passage of the cyclone near the ship and was consistent with the tracks of the cyclone (Fig. 1). After 22/00:00, the lower troposphere became more humid (RH exceeding 80%), while dry air dominated (RH below 10%) above approximately the 300-hPa level and there was accompanying tropopause folding. These observed features were successfully reproduced in CNTL, giving us confidence for further analysis as described below.

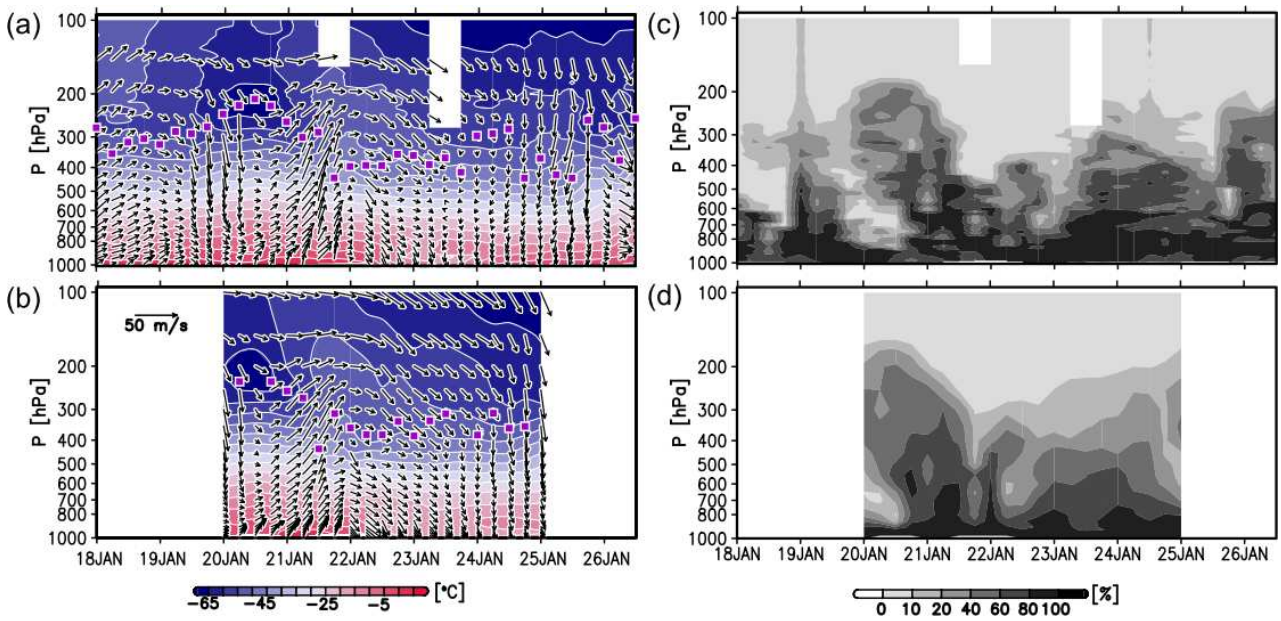

Fig. 3 Pressure–time plots of (a) observed and (b) modelled air temperature and horizontal wind vectors, and (c) observed and (d) modelled RH along the ship transect shown in Fig. 1. Purple squares represent the pressure levels of the tropopause.

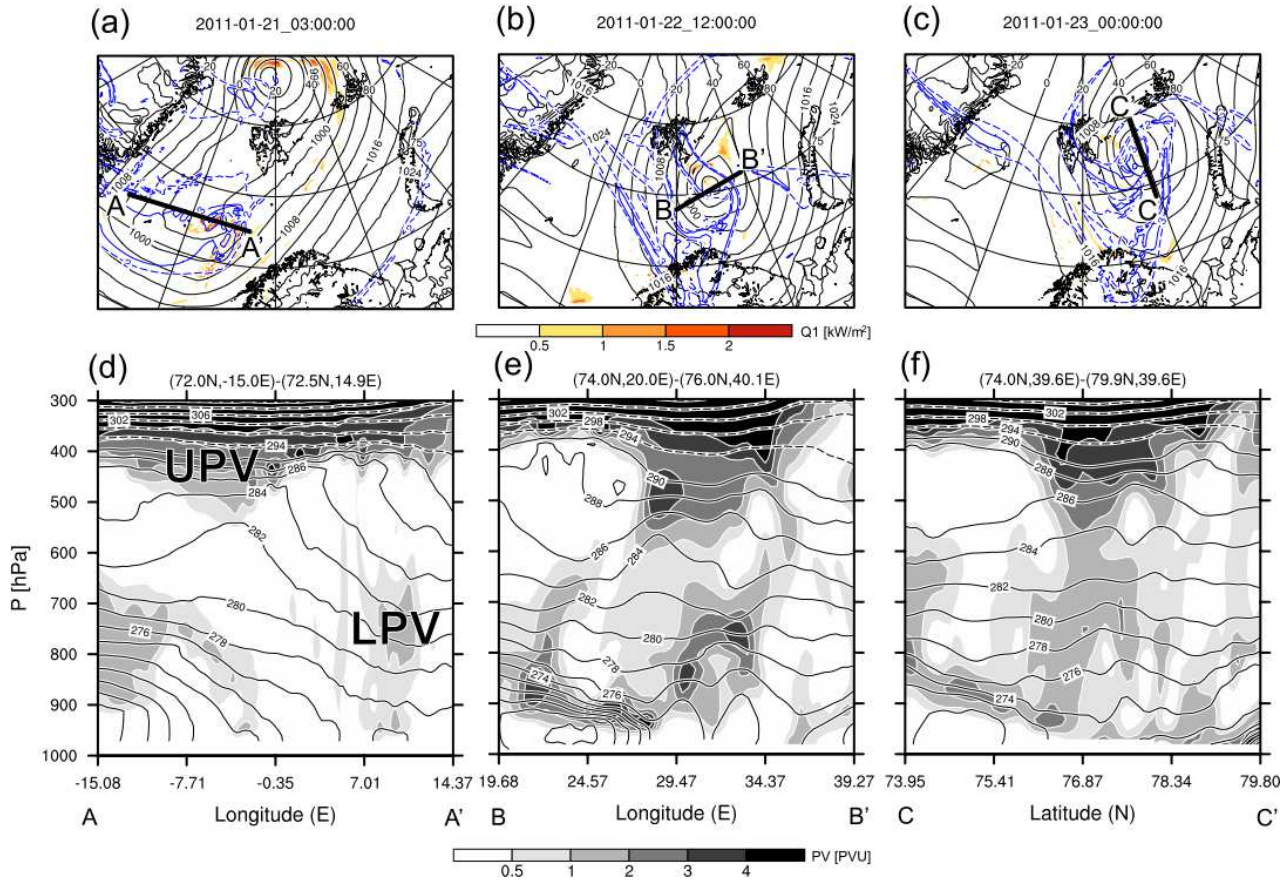

Fig. 4 (Black) Maps of SLP in hPa, (blue) PV at the 300-hPa level in PVU, and (color) vertically integrated condensational heating rate in kWm^{-2} at (a) 21/03:00, (b) 22/12:00, and (c) 23/00:00. Cross sections of (shade) PV and (contour) virtual potential temperature (VPT) along the lines (d) AA´, (e) BB´, and (f) CC´. The contour intervals of the VPT are 2 and 4 K, respectively represented by solid and dashed lines.

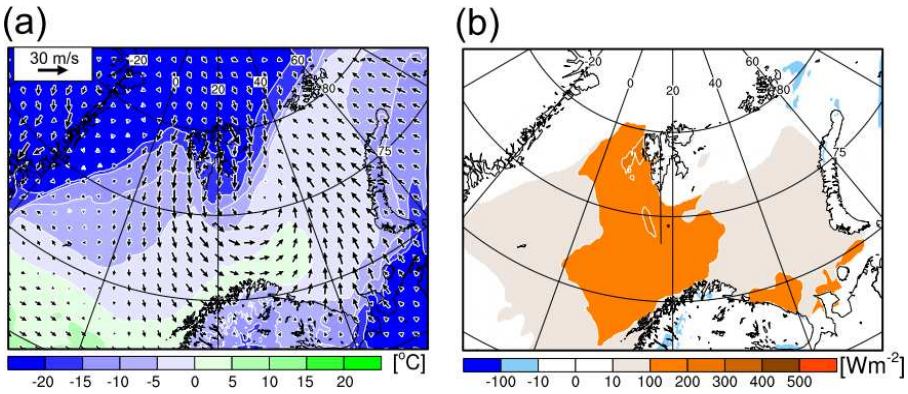

Fig. 5 (a) Maps of (color) SAT and (vector) U_{10} and (b) LHF averaged from 22/00:00 to 23/00:00.

3.2 Life cycle of the cyclone

The cyclone in CNTL initiated north of Iceland and moved towards the east of Svalbard at approximately 21/03:00 (Fig. 4). The cyclone track in CNTL is consistent with that in ERA-Interim data (Fig. 1). The simulated SLP in CNTL was a minimum around 22/00:00 and gradually increased until 24/12:00 (data not shown). The cyclone lasted for more than three days. These features are consistent with satellite infrared images and ERA-Interim data (not shown). During the development phase, air with high values of potential vorticity (PV) exceeding 3 potential vorticity units (PVU; 10^{-6} K m^2 kg^{-1} s^{-1}) at the 300-hPa level extended from Greenland and was located above the surface trough (Fig. 4a, b, d, and e). The vertically integrated condensational heating rate was high east of the surface trough (around the area west of A´ in Fig. 4a). A cross section along the line AA´ shows an upper-tropospheric high-PV anomaly (PV > 1) centered around 4°W and the 400-hPa level (indicated by UPV) while a lower-tropospheric high-PV anomaly (indicated by LPV) dominated east of the upper PV anomaly (Figure 4d). These features (i.e., upper and lower PV anomalies and diabatic heating east of the upper PV anomaly) are consistent with the conditions of Type-C cyclone development proposed by Deveson et al. (2002).

After the development phase, the cyclone moved east of Svalbard and started to decay (Fig. 4c). At the beginning of the mature phase, upper and lower PV anomalies were coupled (Fig. 4f). The cyclone decayed as the upper PV anomaly moved south of the surface cyclone and gradually decoupled with the lower PV anomaly during its mature phase. All the features of the simulated cyclone are consistent with those in the ERA-Interim data (data not shown).

During its mature phase, the cyclone stayed around the ice edge east of Svalbard (Figs. 1 and 4). During this phase, an outbreak of cold air induced by a northerly west of Svalbard due to the cyclone enhanced

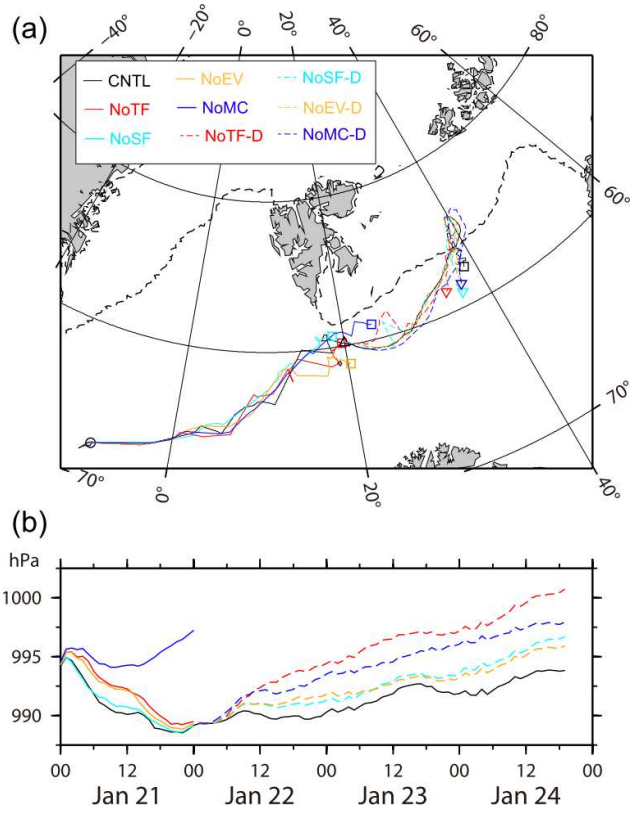

Fig. 6 (a) Tracks of the simulated cyclone and (b) time series of SLP at the storm center. The thick dashed line in (a) indicates the sea-ice edge. Circles in (a) represent the locations of the storm center at 21/00:00. Black and colored squares respectively indicate the locations of the storm center at 25/00:00 and 22/00:00 in CNTL and other experiments (NoTF, NoSF, NoEV, and NoMC). The triangle and inverted triangles respectively indicate the locations of the storm center at 22/00:00 and 24/18:00 in CNTL and the other delayed experiments (NoTF-D, NoSF-D, NoEV-D, and NoMC-D).

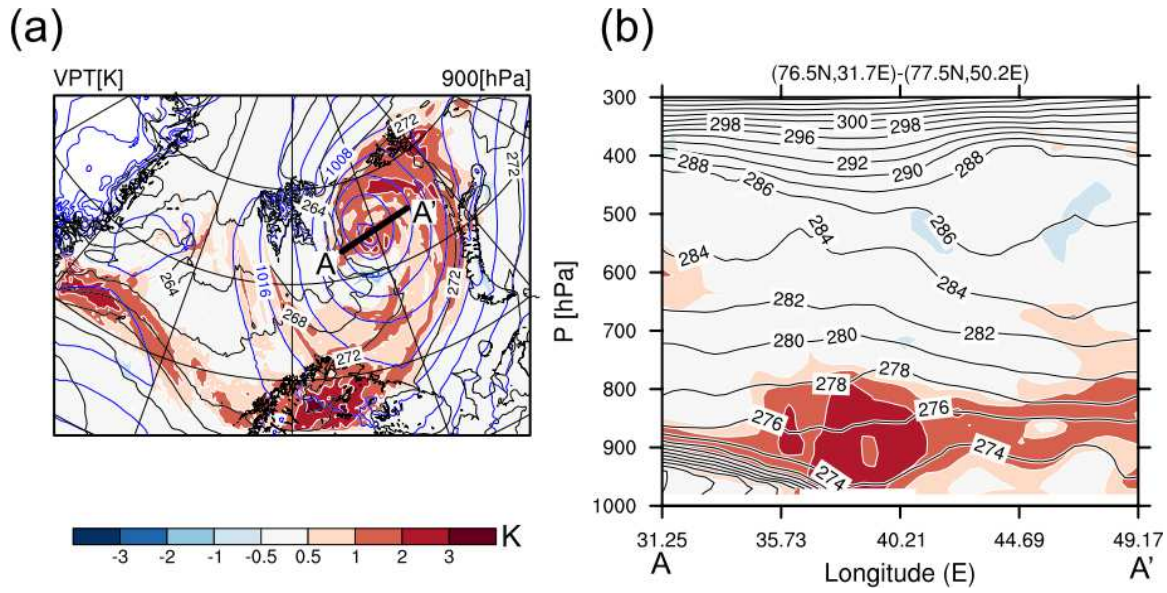

Fig. 7 (a) Map at the 900-hPa level and (b) cross section of differences in VPT between CNTL and NoEV-D in K (color). Black and blue contours represent the VPT in K and SLP in hPa. The thick line AA´ in (a) indicates the location of the cross section in (b).

the surface evaporation (Fig. 5), which may have affected the lifecycle of the cyclone and thermodynamic structure around the cyclone. It is well known that evaporation plays a fundamental role in the life cycle of the tropical cyclone (e.g., Emanuel 2003). However, the development process of the polar cyclone described here is fundamentally different from that of tropical cyclones. The role of evaporation in the life cycle of this cyclone should be different from that in the tropical cyclone and will thus be examined later.

3.3 Sensitivity experiments

Figure 6 shows the track of the cyclone in each sensitivity experiment and time series of the simulated SLP at the storm center. There were no large differences between the tracks of the cyclone in the sensitivity experiments and CNTL. The cyclone hardly deepened when the cloud microphysics and cumulus schemes were switched off during the development phase (NoMC). The SLP at 22/00:00 in NoTF, NoSF, and NoEV was comparable to that in CNTL. In contrast, all the delayed experiments were highly sensitive to the physical processes that were turned off. Condensational heating (NoMC-D) affected the mature phase of the cyclone. NoTF-D saw the strongest effect of the SLP while the effect of turbulent heat flux (NoTF-D) was stronger than that of condensational heating (NoMC-D), which is consistent with the results of Kolstad et al. (2016). The effect of the surface evaporation (NoEV-D) was comparable to that of the surface sensible heat flux (NoSF-D). The effect of the surface evaporation during the mature phase of a cyclone has not been fully addressed in previous studies, and we therefore further examine the results of NoEV-D.

Figure 7 depicts the difference in the virtual potential temperature (VPT) between CNTL and NoEV-D at 23/00:00. CNTL had higher VPT in the lower troposphere around the cyclone than did NoEV-D. Terms in the thermodynamic equation were analyzed to elucidate the dominant processes of this change in VPT.

Figure 8 shows the cross-sections of differences in terms in the thermodynamic equation of the model between CNTL and NoEV-D along the line AA´ in Figure 7a, averaged from 22/01:00 to 23/00:00. The rate of time change in the lower troposphere was positive except in some small areas (Fig. 8a). Local condensational processes dominated the heating in the lower troposphere. Advection also contributed to heating, except near the surface, which is consistent with the results of Screen et al. (2012).

The cloud fraction averaged from 22/01:00 to 23/00:00 (Fig. 9a) indicates the dominance of low-level clouds near the cyclone center. There were also mid-level clouds west of the cyclone center, but changes in cloud fraction were mainly found in the lower troposphere (Fig. 9b), providing evidence for the dominance of condensational heating. In addition, the planetary boundary layer scheme played a role near the surface (Fig. 8e). Longwave radiation counteracted heating except around the 800-hPa level (Fig. 8d). The residual term, relating to physical processes such as horizontal diffusion and shortwave radiation, was negligible (data not shown). The dominance of advection suggests the importance of the remote influence, by which warmer air resulting from diabatic heating is transported from remote areas. The difference

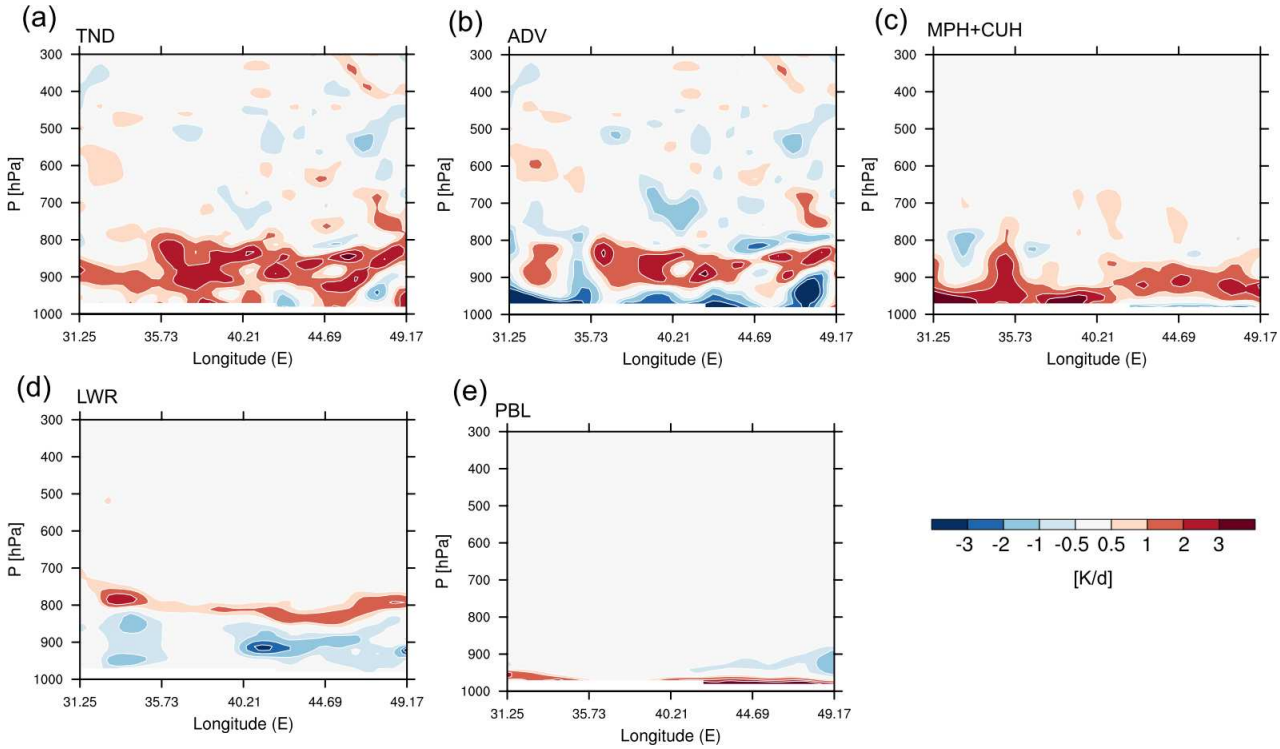

Fig. 8 Cross sections showing differences of terms in the heat budget equation between NoEV-D and CNTL along the line AA´ in Fig. 7a, averaged from 22/01:00 to 23/00:00. (a) Tendency (rate of time change), (b) advection, (c) sum of diabatic heating terms relating to cloud microphysics and cumulus schemes, (d) long-wave radiation, and (e) planetary boundary layer scheme.

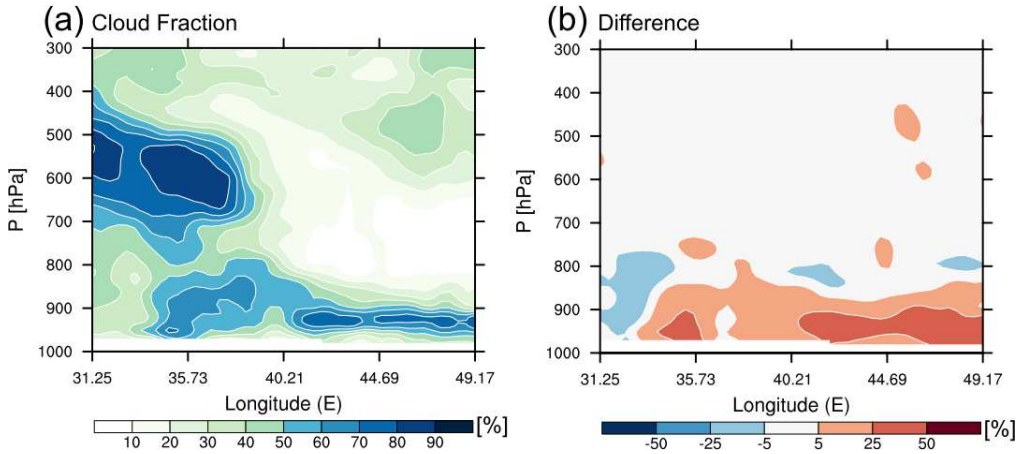

Fig. 9 Cross sections of the cloud fraction in percent: (a) CNTL and (b) difference between NoEV-D and CNTL along the line AA´ in Fig. 7, averaged from 22/01:00 to 23/00:00.

in VPT in Fig. 7(a) suggests the warmer air was created in remote areas around the cyclone and moved into the cyclone center. Trajectory analyses indicate that the VPT of air parcels from around the cyclone near the surface increased, providing evidence of the remote influence (data not shown).

4. Summary and Discussion

The role of surface evaporation in the life cycle of the cyclone and ocean–atmosphere heat exchange in the Barents Sea was investigated through a series of numerical simulations and validated carefully using shipboard surface meteorological observations and atmospheric soundings. An outbreak of cold air and strong winds induced by the cyclone enhanced the surface evaporation during the mature phase of the cyclone. The enhanced evaporation contributed to the longevity of the cyclone. The effect of the surface evaporation was comparable to that of the surface sensible heat flux. An increase in moisture due to surface evaporation caused atmospheric warming in the

lower troposphere over the Barents Sea, as suggested by Inoue and Hori (2011). A detailed thermodynamic analysis revealed that this warming was mainly due to local condensational and boundary layer heating and the advection of warm air.

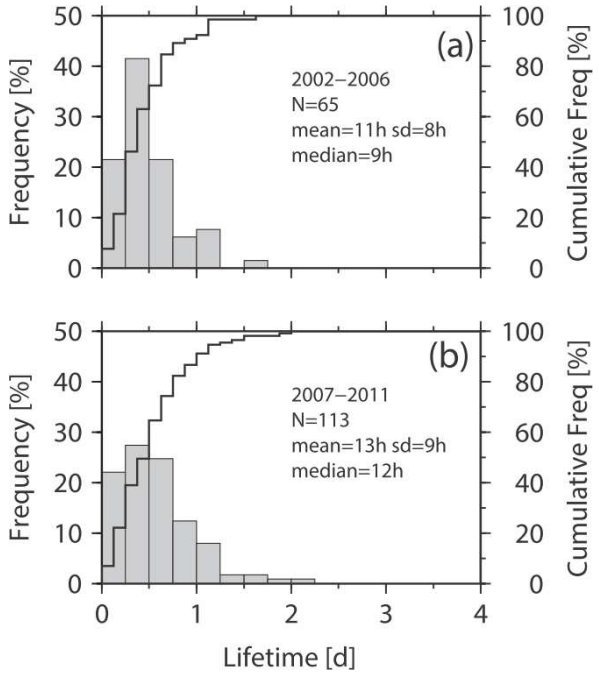

Fig. 10 Histograms of lifetimes of Arctic polar mesocyclones catalogued in the STARS database for (a) 2002–2006 and (b) 2007–2011. Bars and solid lines respectively represent the frequency and cumulative frequency.

Stronger surface winds around the cyclone during the prolonged mature phase should affect the sea-ice distribution. In the sea ice diminishing Arctic, rough seas will contribute to surface evaporation and further contribute to atmospheric warming as shown in this study. Moreover, SST distributions have a rich structure in the Nordic Seas as shown in Fig. 1. The ocean currents should impact such SST distributions and hence the surface evaporation. An interaction between the cyclones and the sea ice distribution and the effect of the sea-ice decline need further investigation because the recent decline in sea ice in the Barents Sea potentially enhances such a warming process.

Although previous studies have paid little attention to the lifetimes of cyclones in the Arctic Ocean (Smirnova et al., 2015), such investigation will be important in the assessment of the effect of cyclones on atmospheric warming in the Arctic. Figure 10 shows histograms of lifetimes of Arctic polar mesocyclones (so-called polar lows) catalogued in the database of Sea Surface Temperature and Altimeter Synergy for Improved Forecasting of Polar Lows (STARS; Eastwood et al., 2012), suggesting an increasing trend in lifetimes. This database does not include cyclones that do not satisfy the definition of a polar low. However, it is worthwhile to expand the lifetime analysis to Arctic cyclones other than polar lows. A long-term trend of the lifetime of cyclones is beyond the scope of this study but should be examined in future research. Continuous monitoring of cyclones is thus an important task. Such monitoring is necessary for the assessment of the long-term change in cyclone characteristics and background environmental parameters (e.g., SST) induced by multidecadal variabilities (Tokinaga et al., 2017) and will contribute to our understanding of the effect of cyclones on Arctic weather and climate. Satellite consternations have been indispensable to study such long-term changes and will continue to be essential for researches in the Arctic climate.

Acknowledgements

The authors thank R. Ingvaldsen and the crews of R/V Johan Hjort of the Institute of Marine Research, Norway, and participants in the field campaign for their help with data collection. The authors also thank K. Hines and the Polar Meteorology Group, Byrd Polar and Climate Research Center, Ohio State University for providing Polar WRF. Constructive comments from two anonymous reviewers and fruitful discussion with W. Yanase, U. Shimada, and S. Watanabe are greatly appreciated. This manuscript was edited by Glenn Pennycook from Edanz Group. This work was supported in part by the Arctic Challenge for Sustainability and the Japan Society for Promotion for Science through Grants-in-Aid for Scientific Research (16H01844, 16H04046, 17H02958, 18H03745, 18KK0292, and 19H05697).

References

Adakudlu, M. and I. Barstad (2011): Impacts of the ice-cover and sea-surface temperature on a polar low over the Nordic seas: a numerical case study. *Q.J.R. Meteorol. Soc.*, **137**: 1716-1730.

Boisvert L.N., D.L. Wu and C.L. Shie (2015): Increasing evaporation amounts seen in the Arctic between 2003 and 2013 from AIRS data. *J. Geophys. Res.*, **120**: 6865–6881.

Boisvert, L.N., A.A. Petty and J.C. Stroeve (2016): The impact of the extreme winter 2015/16 Arctic cyclone on the Barents -Kara Seas. *Mon. Wea. Rev.*, **144**: 4279 – 4287.

Dai, A., D. Luo and 2 others (2019): Arctic amplification is caused by sea-ice loss under increasing CO_2. *Nat. Comm.*, **10**: 121, https://doi.org/10.1038/s41467-018-07954-9.

Dee, D.P., S.M. Uppala and 34 others (2011): The ERA-Interim reanalysis: configuration and performance of the data assimilation system. *Q.J.R. Meteorol. Soc.*, **137**: 553–597.

Deser, C., R. Tomas, M. Alexander and D. Lawrence (2010): The seasonal atmospheric response to projected Arctic sea ice loss in the late twenty-first century. *J. Clim.*, **23**: 333–351.

Deveson, A.C., K.A. Browning and T.D. Hewson (2002): A classification of FASTEX cyclones using a height-attributable quasi-geostrophic vertical-motion diagnostic. *Q.J.R. Meteorol.*

Soc., **128**: 93-117.
Dudhia, J. (1989): Numerical study of convection observed during the Winter Monsoon Experiment using a mesoscale two-dimensional model. *J*. *Atmos*. *Sci*., **46**: 3077–3107.
Dufour, A., O. Zolina and S. K. Gulev (2016): Atmospheric moisture transport to the Arctic: Assessment of reanalyses and analysis of transport components. *J*. *Clim.*, **29**: 5061-5081.
Eastwood, S., Y. Gusdal and 4 others (2012): *STARS-DAT v3 user manual version 3.1*. Norwegian Meteorological Institute, Oslo, Norway, 40 pp.
Emanuel, K. (2003): Tropical Cyclones. *Annual Review of Earth and Planetary Sciences*, **31**: 75-104.
Føre, I., J.E. Kristjánsson and 4 others (2012): A 'hurricane-like' polar low fuelled by sensible heat flux: high-resolution numerical simulations. *Q*.*J*.*R*. *Meteorol*. *Soc*., **138**: 1308–1324.
Hao, M., Y. Luo, Y. Lin, Z. Zhao and 2 others (2019): Contribution of atmospheric moisture transport to winter Arctic warming. *Int*. *J*. *Climatol*., **39**: 2697– 2710.
Hines, K.M. and D.H. Bromwich (2008): Development and testing of polar weather research and forecasting (WRF) model. Part I: Greenland ice sheet meteorology. *Mon*. *Wea*. *Rev*., **136**: 1971-1989.
Hong, S.Y., Y. Noh and J. Dudhia (2006): A new vertical diffusion package with an explicit treatment of entrainment processes. *Mon*. *Wea*. *Rev*., **134**: 2318–2341.
Inoue, J. and M.E. Hori (2011): Arctic cyclogenesis at the marginal ice zone: A contributory mechanism for the temperature amplification? *Geophys*. *Res*. *Lett*., **38**: L12502, https://doi.org/10.1029/2011GL047696.
Kain, J.S. (2004): The Kain-Fritsch convective parameterization: an update. *J*. *Appl*. *Meteor*., **43**: 170–181.
Kolstad, E.W., T.J. Bracegirdle and M. Zahn (2016): Re-examining the roles of surface heat flux and latent heat release in a "hurricane-like" polar low over the Barents Sea. *J*. *Geophys*. *Res*., **121**: 7853‐ 7867.
Mlawer, E.J., S.J. Taubman and 3 others (1997): Radiative transfer for inhomogeneous atmospheres: RRTM, a validated correlated-k model for the longwave. *J*. *Geophys*. *Res*., **102**: 16663-16682.
Moore, G.W.K. (2016): The December 2015 North Pole warming event and the increasing occurrence of such events. *Sci*. *Rep*., **6**: 1-11.
Morrison, H., G. Thompson and V. Tatarskii (2009): Impact of cloud microphysics on the development of trailing stratiform precipitation in a simulated squall line: comparison of one- and two-moment schemes. *Mon*. *Wea*. *Rev*., **137**: 991-1007.
Nakanishi, M. and H. Niino (2009): Development of an improved turbulence closure model for the atmospheric boundary layer. *J*. *Meteorol*. *Soc*. *Jpn*., **87**: 895-912.
Reynolds, R.W., T.M. Smith and 4 others (2007): Daily high-resolution-blended analyses for sea surface temperature. *J*. *Clim*., **20**: 5473–5496.
Screen, J.A. and I. Simmonds (2010): The central role of diminishing sea ice in recent Arctic temperature amplification. *Nature*, **464**: 1334–1337.
Screen, J.A., C. Deser and I. Simmonds (2012): Local and remote controls on observed Arctic warming, *Geophys*. *Res*. *Lett*., **39**: L10709, doi:10.1029/2012GL051598.
Serreze, M.C. (1995): Climatological aspects of cyclone development and decay in the Arctic, *Atmosphere-Ocean*, **33**: 1-23, https://doi.org/10.1080/07055900.1995.9649522.
Skamarock, W.C., J.B. Klemp and 7 others (2008): A description of the Advanced Research WRF Version 3. *NCAR technical note NCAR/TN-475+STR*, NCAR: Boulder, Colorado, USA, 113pp., doi: 10.5065/D68S4MVH.
Smirnova, J.E., P.A. Golubkin and 3 others (2015): Polar low climatology over the Nordic and Barents seas based on satellite passive microwave data. *Geophys*. *Res*. *Lett*., **42**: 5603-5609.
Tokinaga, H., S.P. Xie and H. Mukougawa (2017): Early 20th-century Arctic warming intensified by Pacific and Atlantic multidecadal variability, *Proc*. *Nat*. *Acad*. *Sci*. **114**, 6227-6232.
Zahn, M., M. Akperov and 3 others (2018) Trends of cyclone characteristics in the Arctic and their patterns from different reanalysis data. *J*. *Geophys*. *Res*., **123**: 2737-2751.

Summary in Japanese

和文要約

低気圧を媒介とした北極海における海洋ー大気間の熱交換のメカニズム： 2011 年 1 月にバレンツ海で観測された低気圧の事例解析

万田敦昌 [1], 三井拓 [2], 猪上淳 [2, 3], 堀正岳 [3, 4], 河本和明 [5], 小松謙介 [1]

[1] 三重大学, [2] 総合研究大学院大学, [3] 国立極地研究所, [4] 海洋研究開発機構, [5] 長崎大学

北極温暖化における低気圧の果たす役割の重要性が近年の研究で指摘されている。既往の多くの研究は中緯度からの顕熱・潜熱の水平輸送に焦点を当てており，北極海の蒸発の影響に着目したものは無い。そこで 2011 年 1 月にバレンツ海で行われた現地観測で捉えられた低気圧を対象として，海面からの蒸発が低気圧に及ぼす影響を数値シミュレーションによって調べた。海面からの蒸発は，低気圧の長寿命化に寄与し，その効果は顕熱と同程度であった。熱収支解析から海面からの蒸発は凝結加熱，境界層における加熱，および暖気移流の強化を通じて，気温を上昇させていることが明らかとなった。近年の海氷減少とそれに伴う蒸発の強化は，本研究で示された低気圧を媒介とした海洋ー大気間の熱交換を促進し，北極海のさらなる温暖化に寄与している可能性がある。